Oxygen Transport Ceramic Membranes

Quarterly Report

April 2006 – June 2006

Principal Authors:

Prof. S. Bandopadhyay

Dr. T. Nithyanantham

Issued: July 2006

University of Alaska Fairbanks
Fairbanks, AK 99775

Contributing Authors:

1. **Y-W. Sin and H. U. Anderson,** Materials Research Center, University of Missouri-Rolla, Rolla, MO 65401

2. **Prof. Alan Jacobson and Prof. C.A. Mims;** University of Houston/University of Toronto

DISCLAIMER

This report was prepared as an account of the work sponsored by an agency of the United States Government. Neither the United States Government nor any agency thereof, nor any of their employees, makes any warranty, express or implied, or assumes any legal liability or responsibility for the accuracy, completeness, or usefulness of any information, apparatus, product, or process disclosed, or represents that its use would not infringe privately owned rights. Reference herein to any specific commercial product, process, or service by trade name, trademark, manufacturer, or otherwise does not necessarily constitute or imply its endorsement, recommendation, or favoring by the United States Government or any agency thereof. The views and opinions of authors expressed herein do not necessarily state or reflect those of the United States Government or any agency thereof.

ABSTRACT

A non-agglomerated and nanocrystalline-sized powder was successfully produced using ethylene glycol nitrate methods. The LSFT powder prepared using this method exhibits well dispersed and nano sized particles about 100 – 200 nm. The density of LSFT sintered at $1300^{o}C$ was about 90% of the theoretical density at which is $100^{o}C$ less than that of the previous LSFT which was sintered at $1400^{o}C$. The sample sintered at $1400^{o}C$ exhibited the evidence of a liquid phase at the grain boundaries and 2nd phase formation which probably caused low mechanical stability. The electrical conductivity and Seebeck coefficient were measured as a function of temperature.

The LSFT-CGO specimens were cut from the as sintered bars and used for the evaluation of Mechanical Properties after polishing. The effect of strain rate on the flexural strength of the LSFT-CGO test specimens was studied. Three strain rates 6, 60 and 600 μm/ min were chosen for this study. It is observed from the results that with increasing cross head speed the membrane takes higher loads to fail. A reduction in the strength of the membrane was observed at 1000°C in N_2.

Two different routes were investigated to synthesis GDC using either formate or carbonate precursors. The precursor and CGO particle morphologies were examined by scanning electron microscopy. The thermal decomposition behaviors of $Ce(Gd)(HCOO)_3$ and $Ce(Gd)(CO_3)(OH)$ were determined by thermogravimetric analysis (TGA) at a rate of $3^{°}C/min$ in air. The X-ray powder diffraction patterns of the precursor and CGO were collected and nitrogen adsorption isotherms were measured. Conductivity measurements were made by AC impedance spectroscopy on sintered disks in air using platinum electrodes.

TABLE OF CONTENTS

LIST OF GRAPHICAL MATERIALS

LIST OF TABLES

INTRODUCTION

Conversion of natural gas to liquid fuels and chemicals is a major goal for the Nation as it enters the 21st Century. Technically robust and economically viable processes are needed to capture the value of the vast reserves of natural gas on Alaska's North Slope, and wean the Nation from dependence on foreign petroleum sources. Technologies that are emerging to fulfill this need are all based syngas as an intermediate. Syngas (a mixture of hydrogen and carbon monoxide) is a fundamental building block from which chemicals and fuels can be derived. Lower cost syngas translates directly into more cost-competitive fuels and chemicals.

The currently practiced commercial technology for making syngas is either steam methane reforming (SMR) or a two-step process involving cryogenic oxygen separation followed by natural gas partial oxidation (POX). These high-energy, capital-intensive processes do not always produce syngas at a cost that makes its derivatives competitive with current petroleum-based fuels and chemicals.

In the mid 80's BP invented a radically new technology concept that will have a major economic and energy efficiency impact on the conversion of natural gas to liquid fuels, hydrogen, and chemicals.[1] This technology, called Electropox, integrates oxygen separation with the oxidation and steam reforming of natural gas into a single process to produce syngas with an economic advantage of 30 to 50 percent over conventional technologies.[2]

The Electropox process uses novel and proprietary solid metal oxide ceramic oxygen transport membranes [OTMs], which selectively conduct both oxide ions and electrons through their lattice structure at elevated temperatures.[3] Under the influence of an oxygen partial pressure gradient, oxygen ions move through the dense, nonporous membrane lattice at high rates with 100 percent selectivity. Transported oxygen reacts with natural gas on the fuel side of the ceramic membrane in the presence of a catalyst to produce syngas.

In 1997 BP entered into an OTM Alliance with Praxair, Amoco, Statoil and Sasol to advance the Electropox technology in an industrially sponsored development program. These five companies

[1]Mazanec, T. J.; Cable, T. L.; Frye, J. G., Jr.; US 4,793,904, 27 Dec **1988**, assigned to The Standard Oil Company (now BP America), Mazanec, T. J.; Cable, T. L.; US 4,802,958, 7 Feb **1989**, assigned to the Standard Oil Co. (now BP America), Cable, T. L.; Mazanec, T. J.; Frye, J. G., Jr.; European Patent Application 0399833, 24 May **1990**, published 28 November **1990.**

[2]Bredesen, R.; Sogge, J.; "A Technical and Economic Assessment of Membrane Reactors for Hydrogen and Syngas Production" presented at Seminar on the Ecol. Applic. of Innovative Membrane Technology in the Chemical Industry", Cetraro, Calabria, Italy, 1-4 May **1996**.

[3] Mazanec, T.J., *Interface*, **1996**; Mazanec, T.J., *Solid State Ionics*, 70/71, **1994** 11-19; "Electropox: BP's Novel Oxidation Technology", T.J. Mazanec, pp 212-225, in "The Role of Oxygen in Improving Chemical Processes", M. Fetizon and W.J. Thomas, eds, Royal Society of Chemistry, London, **1993**; "Electropox: BP's Novel Oxidation Technology", T.J. Mazanec, pp 85-96, in "The Activation of Dioxygen and Homogeneous Catalytic Oxidation", D.H.R. Barton, A. E. Martell, D.T. Sawyer, eds, Plenum Press, New York, **1993**; "Electrocatalytic Cells for Chemical Reaction", T.J. Mazanec, T.L. Cable, J.G. Frye, Jr.; Prep Petrol Div ACS, San Fran, **1992** *37*, 135-146; T.J. Mazanec, T.L. Cable, J.G. Frye, Jr.; *Solid State Ionics*, **1992**, 53-56, 111-118.

have been joined by Phillips Petroleum and now are carrying out a multi-year $40+ million program to develop and commercialize the technology. The program targets materials, manufacturing and engineering development issues and culminates in the operation of semi-works and demonstration scale prototype units.

The Electropox process represents a truly revolutionary technology for conversion of natural gas to synthesis gas not only because it combines the three separate unit operations of oxygen separation, methane oxidation and methane steam reforming into a single step, but also because it employs a chemically active ceramic material in a fundamentally new way. On numerous fronts the commercialization of Electropox demands solutions to problems that have never before been accomplished. Basic problems in materials and catalysts, membrane fabrication, model development, and reactor engineering all need solutions to achieve commercial success. Six important issues have been selected as needing understanding on a fundamental level at which the applied Alliance program cannot achieve the breadth and depth of understanding needed for rapid advancement. These issues include:

1. Oxygen diffusion kinetics (University of Houston);
2. Phase stability and stress development (University of Missouri - Rolla);
3. Mechanical property evaluation in thermal and chemical stress fields (University of Alaska Fairbanks)

Statement of Work

Task 1   *Evaluate phase stability and thermal expansion of candidate perovskite membranes and develop techniques to support these materials on porous metal structures.*

Task 2   *Determine materials mechanical properties under conditions of high temperatures and reactive atmospheres.*

Task 3   *Measure kinetics of oxygen uptake and transport in ceramic membrane materials under commercially relevant conditions using isotope labeling techniques.*

EXECUTIVE SUMMARY

The LSFT powder prepared using ethylene glycol nitrate method exhibits well dispersed and nano sized particles about 100 – 200 nm. The density of LSFT sintered at 1300°C was about 90% of the theoretical density at which is 100°C less than that of the previous LSFT which was sintered at 1400°C. The sample sintered at 1400°C exhibited the evidence of a liquid phase at the grain boundaries and 2nd phase formation which probably caused low mechanical stability. The electrical conductivity and Seebeck coefficient were measured as a function of temperature.

The effect of strain rate on the flexural strength of the LSFT-CGO test specimens was studied. It is observed from the results that with increasing cross head speed the membrane takes higher loads to fail. A reduction in the strength of the membrane was observed at 1000°C in N_2. It was identified from the bend strength experiments that the geometry plays an important role in achieving proper fracture of the sample.

GDC was prepared using either formate or carbonate precursors. The precursor and CGO particle morphologies were examined by scanning electron microscopy. The thermal decomposition behaviors of $Ce(Gd)(HCOO)_3$ and $Ce(Gd)(CO_3)(OH)$ were determined by thermogravimetric analysis. The XRD patterns of the precursor and CGO were collected and nitrogen adsorption isotherms were measured. Conductivity measurements were made by AC impedance spectroscopy on sintered disks in air using platinum electrodes.

Task 1:   **Preparation and Characterization of Dense Ceramic oxygen Permeable Membranes**

Yong-Wook Sin and H. U. Anderson

**Materials Research Center, University of Missouri-Rolla, Rolla, MO 65401**

Conductivity and Seebeck coefficient of $La_{0.2}Sr_{0.8}Fe_{0.55}Ti_{0.45}O_{3-\delta}$ (LSFT) as a function of temperature

UMR has recently developed an improved method for preparation of multi-component powder systems. The method was used to prepare LSFT ($La_{0.2}Sr_{0.8}Fe_{0.55}Ti_{0.45}O_{3-\delta}$) nanocrystalline powder. Several water based solution processes were tested to prepare well dispersed and nano sized LSFT powder. Among them, the method using ethylene glycol and nitrates produced the best nanocrystalline LSFT powder. The new LSFT sample was prepared using this new LSFT powder and was characterized by using XRD, optical microscope, and SEM. The electrical conductivity and Seebeck coefficient as a function of temperature were also measured in air.

Results and Discussion

Several different, water based chemical preparation methods using glycine, sucrose and ethylene glycol were used to prepare LSFT powders. A non-agglomerated and nanocrystalline-sized powder was successfully produced using ethylene glycol nitrate methods. The density of LSFT sintered at 1300°C was about 90% of the theoretical density at which is 100°C less than that of the previous LSFT which was sintered at 1400°C. Figure 1 shows optical photomicrographs of the powder previously prepared

4

using the glycine nitrate process and the currently prepared LSFT powders using the ethylene glycol nitrate method.
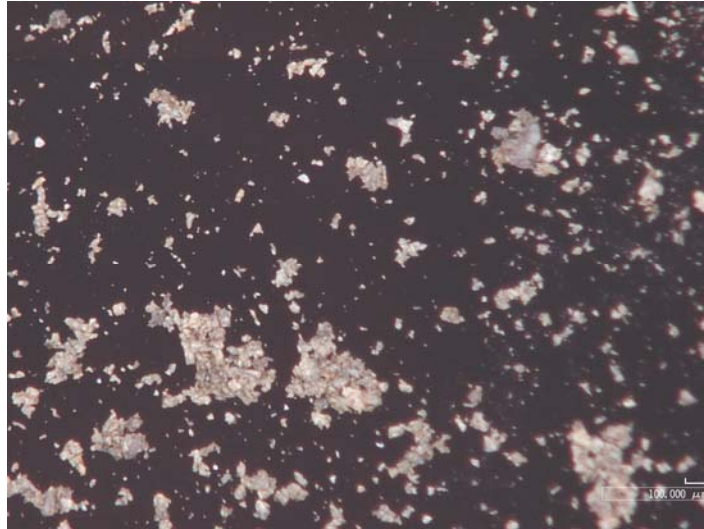
(a) Previously prepared LSFT powder using glycine nitrate method
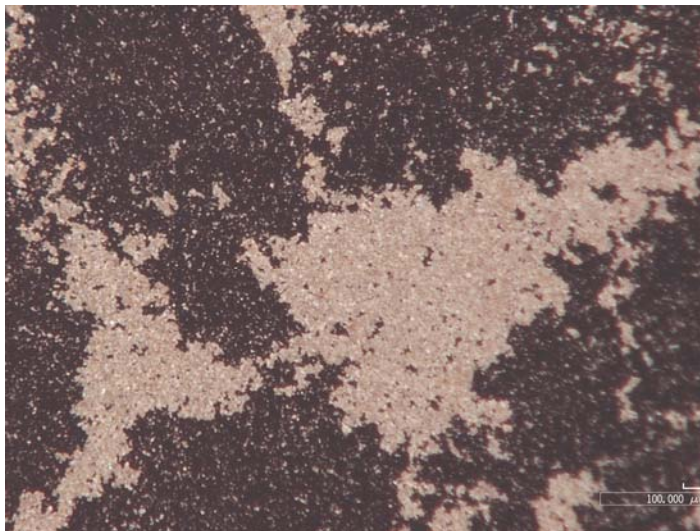
(b) Newly prepared LSFT powder using ethylene glycol nitrate method

Figure 1.   Optical micrographs of the LSFT powder was prepared using (a) glycine-nitrate method and (b) ethylene glycol nitrate method

As can be seen in these figures, the LSFT powder prepared using glycine nitrate method shows agglomerated large particle size of about 10 – 20 μm. On the other hand, the LSFT powder prepared using ethylene glycol nitrate method exhibits well dispersed and nano sized particles about 100 – 200 nm. Figure 1 (b) appeared to have large agglomerates of LSFT particles even though the particles were actually well dispersed. This is due to the drying process of alcohol during the powder sample preparation for optical microscopy. The LSFT powder was agglomerated on the cover glass during the drying process of alcohol. The prepared LSFT nano powder was pressed using uni-axial press with about 200 MPa followed by sintering at 1200, 1300 and 1400°C to investigate the optimum sintering temperature.

Figure 2 shows the SEM micrographs of the new LSFT samples from the different sintering temperatures. As can be seen in the figures, LSFT sample sintered at 1200°C exhibited large pores all over the sample surface. Due to the low sinterability, the mechanical strength of this sample was low and could be broken by hand. However, the LSFT sample sintered at 1300°C showed no visible pores on the surface of the sample and had 90% of the theoretical density and no evidence of the 2nd phase formation. On the other hand, the LSFT sample sintered at 1400°C exhibited the evidence of a liquid phase at the grain boundaries and 2nd phase formation which probably caused low mechanical stability. Actually, the 1400°C sample shattered during the sintering process. (1400°C was the optimum sintering temperature for the previous LSFT sample) The mechanical instability of the sample sintered at 1400°C probably is due to the mismatch of thermal expansion coefficients between the different phases formed during the sintering process. Corresponding X-ray results were shown in Figure 3. However,

according to the X-ray results, there was no evidence of the 2nd phase formation at 1400°C. Actually there was no difference between XRD results from the samples sintered from 1200, 1300 and some minor peaks disappeared at 1400°C. However, 1400°C was too high because a liquid was formed at that temperature. Therefore, the optimum sintering temperature should have been somewhere between 1300 and 1400°C. The chemical analysis will be carried out on the samples to investigate the discrepancy of results between SEM and XRD.
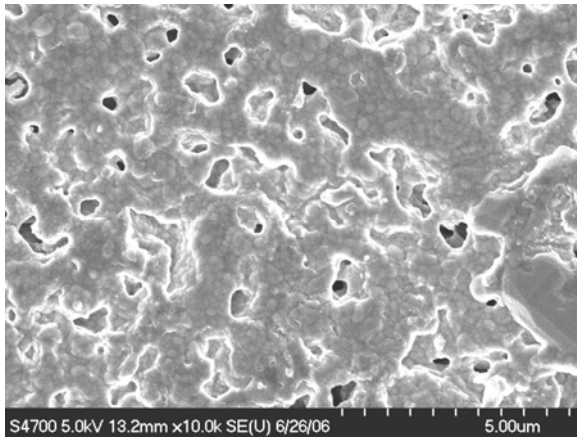
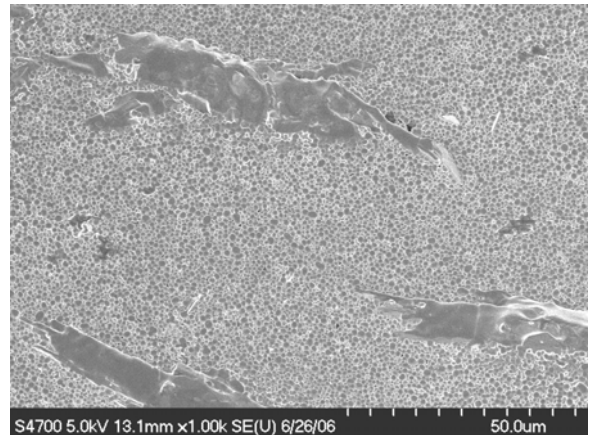(a) LSFT sintered at 1200°C in air
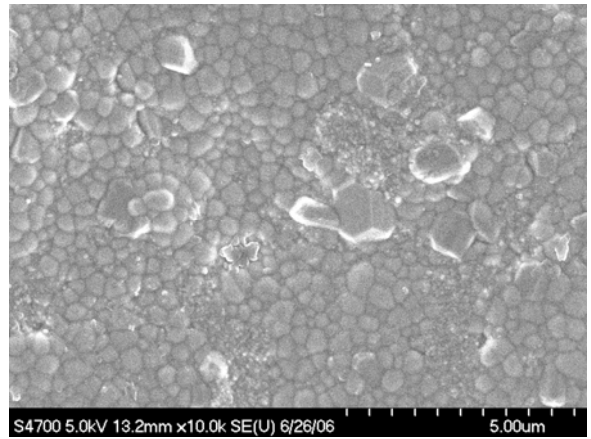
(b) LSFT sintered at 1300°C in air
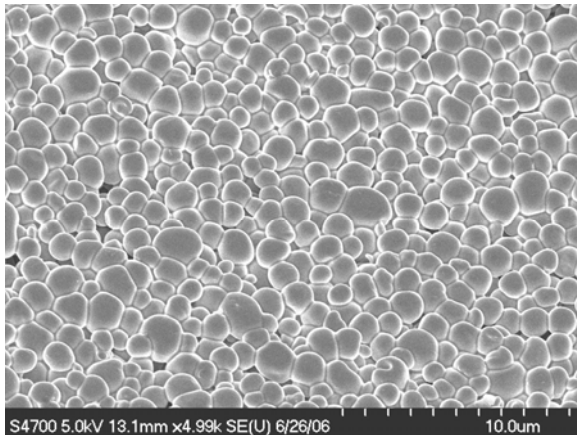
(c) LSFT sintered at 1400°C in air

(d) LSFT sintered at 1400°C in air but different scale

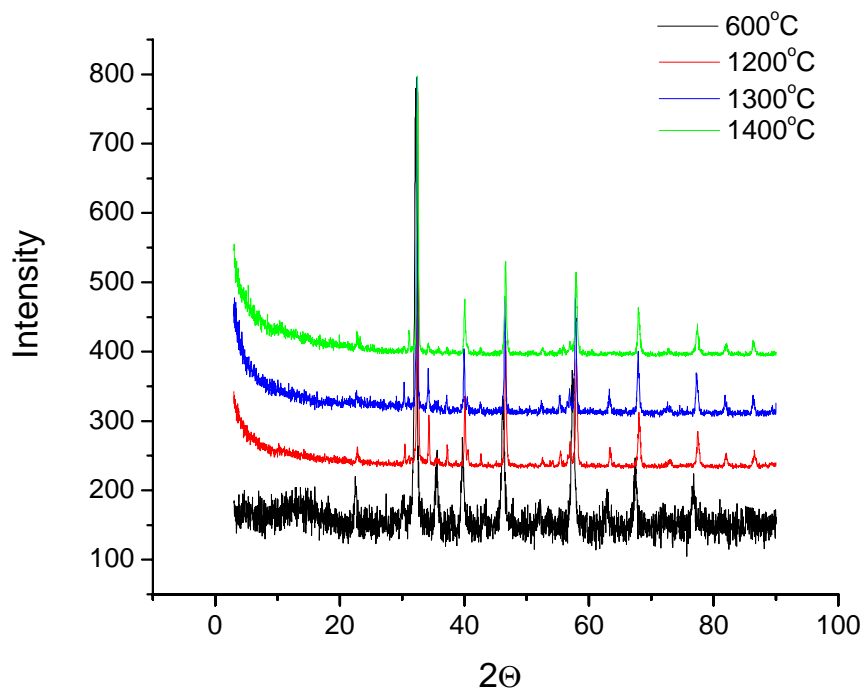Figure 2. SEM micrograph of LSFT at different sintering temperature in air

Figure 3. XRD profiles of LSFT annealed at 600, 1200, 1300, and 1400°C

The electrical conductivity and thermoelectric power were measured in air on the LSFT sample sintered at 1300°C. As can be seen in Figure 4, the conductivity increased with temperature up to 800°C and then became essentially constant up to the temperature of 1200°C. If the mobility dominated the conductivity process, the conductivity should have steadily increased with increasing temperature. Obviously this is not the case. It appears from the Seebeck coefficient data which are also shown in Figure 4, the carrier concentration increases with increasing temperature which suggests that the acceptor concentration increased. This may be due to changes in the valence states of Ti and Fe as temperature increased. Above 700°C, the Seebeck Coefficient decreased to the point that the sensitivity of voltmeter being used for the thermoelectric voltage measurement

was exceeded, so any data above that temperature are suspect. However, it is apparent that the Seebeck Coefficients became essentially constant with further increases of temperature. This suggests that the carrier concentration became constant which could be an explanation of the behavior of the conductivity. That is; i) at low temperatures, the carrier concentration increased thereby accelerating an increase in the conductivity beyond that due to the mobility term and ii) at temperatures above 700^oC the carrier concentration tended to be constant which caused increases in conductivity to be smaller. However, more investigation needs be performed on this new LSFT material to explain more about these behaviors.
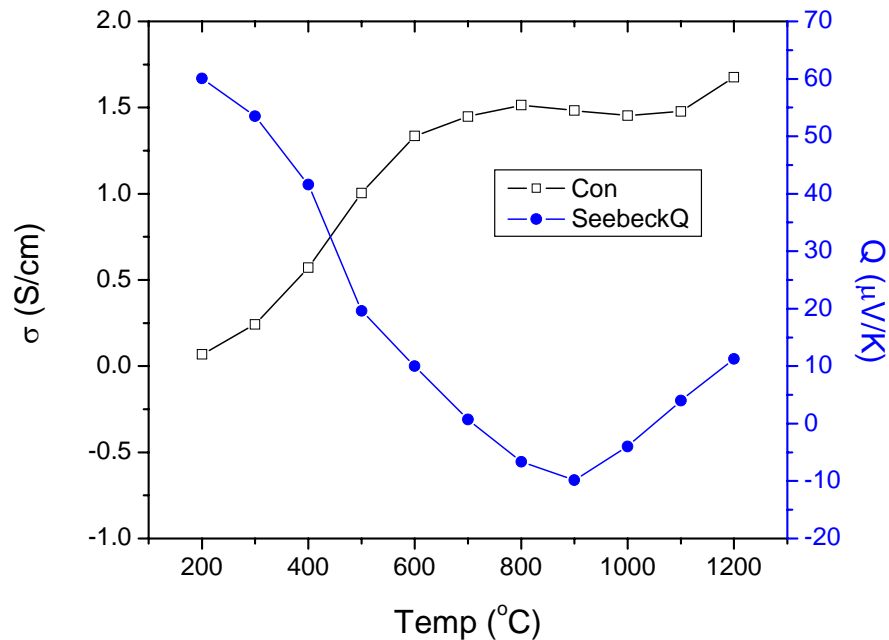

Figure 4.   The electrical conductivity and Seebeck coefficient were measured as a function of temperature

Future Work

1. The powder preparation process should be optimized.

2. More measurements of electrical conductivity and Seebeck coefficient will be carried out as a function of temperature and oxygen activity

3. The chemical analysis on the LSFT sample will be carried out.

4. Carrier concentration, mobility of charge carrier, and net acceptor dopant concentration will be estimated which will allow explanation of the behavior of the electrical conductivity.

Determine material mechanical properties under conditions of high temperature and reactive atmosphere

Prof. S. Bandopadhyay and Dr. T. Nithyanantham

University of Alaska Fairbanks, AK 99775

Experimental:

The LSFT-CGO specimens were cut from the as sintered bars and used for the evaluation of Mechanical Properties after polishing. The sample preparation methods were discussed in the previous report (OTM, Quarterly report. Page 4, Jan-March 2006). The figure 5 shows the photograph of the as-sintered and test specimen.
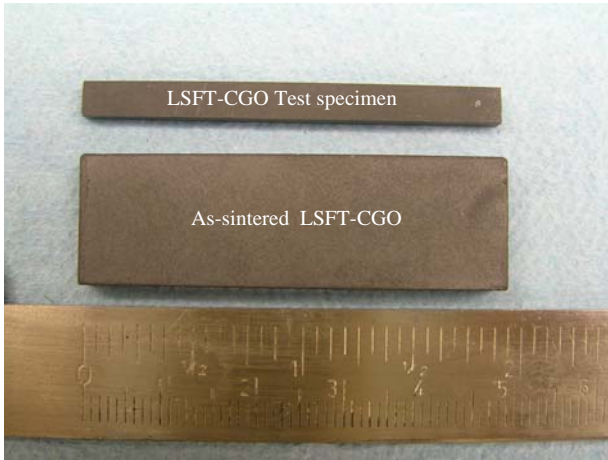

Figure 5. Photographs of as-sintered and test specimens.

The effect of strain rate on the flexural strength of the LSFT-CGO test specimens was studied. Three strain rates 6, 60 and 600 μm/ min were chosen for this study. The samples were mounted in 4-point bend test fixture and the load was applied with the strain rate mentioned until the specimen fractures. The load-deflection data was plotted and analyzed. The fracture surfaces after the test was secured for further analysis using SEM, XRD and thermal analysis.

High density alumina test specimens with the same dimensions were also prepared with a notch in the middle of the bars and used for calibration purposes.

The flexural strength was calculated using the simple beam formula,

$$\text{Fracture strength } \sigma_f, \text{ MPa} = \left(\frac{3PL}{4BW^2} \right) \quad \text{--- (2.1)}$$

Where P = Fracture Load (N)

L= Outer Span (here 3.81 cm)

B= thickness and

W= width of the beam respectively.

Results and Discussion:

Figure 6 shows the LSFT-CGO flexural strength, tested at the strain rate of 6 μm/min at RT in air. It is observed that there is monotonic increase in the load till the specimen fails at the maximum load.
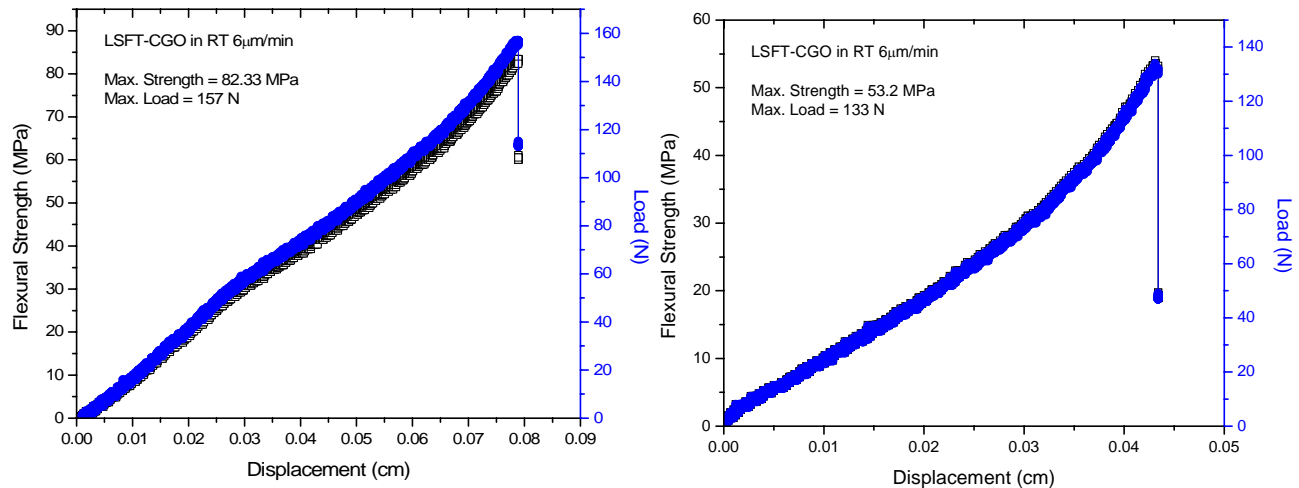

Figure 6. LSFT-CGO Flexural strength tested at the strain rate of 6 μm/min. at RT in air.

The maximum strength values that ware calculated for the two LSFT-CGO bars fractured at 6μm/min were 82.3 and 53.2 MPa respectively. The scattering in the values or the difference between these two values are relatively higher. This may be due to the

size of critical flaw or experimental problems. In order to understand the effect of strain rate on the LSFT-CGO samples, next strain rate (60μm/min) was employed. The Figure 7 shows the LSFT-CGO Flexural strength tested at the strain rate of 60 μm/min at RT in air.
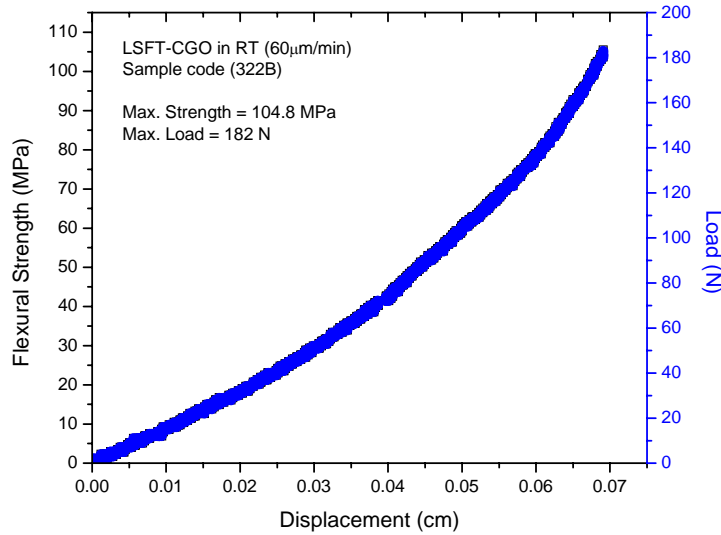

Figure 7. LSFT-CGO Flexural strength tested at the strain rate of 60 μm/min. at RT in air.

In the Figure 7 the maximum strength value was calculated as 104.8 MPa and the fracture load was found to be 182 N. It is observed that the fracture load at 60μm/min is higher than at 6μm/min. The flexural strength tests at the strain rate of 600 μm/ min were carried out and the results were plotted in Figure 8. As observed in the previous experiments with slower strain rates, the increasing load leads to failure at 201 and 219 N. The flexural strength values calculated from the loads were 94.1 MPa and 90.8 MPa respectively.

The flexural strength results are summarized in the Table 1 and load-displacement curves of three selected specimens were shown in Figure 9. It is observed from the results that with increasing cross head speed the membrane takes higher loads to fail. This kind of fracture behavior is quite normal in the flaw containing brittle materials.
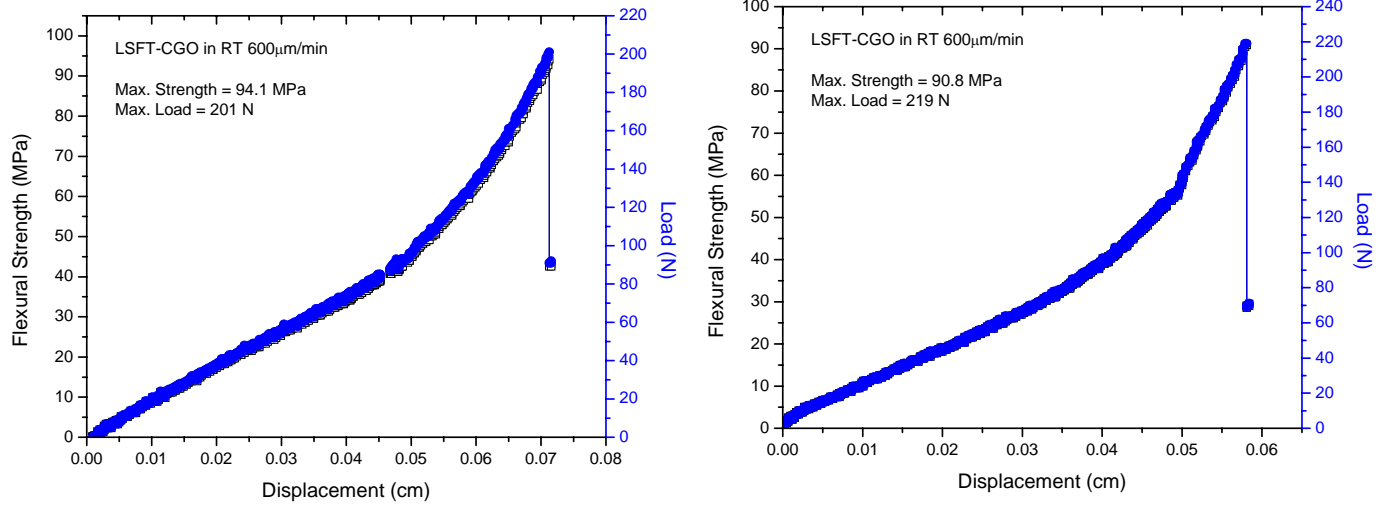
Figure 8. LSFT-CGO Flexural strength tested at the strain rate of 600 μm/min. at RT in air.

Table 1. LSFT-CGO Flexural strength tests at RT and at 1000°C in N_2 atmosphere.

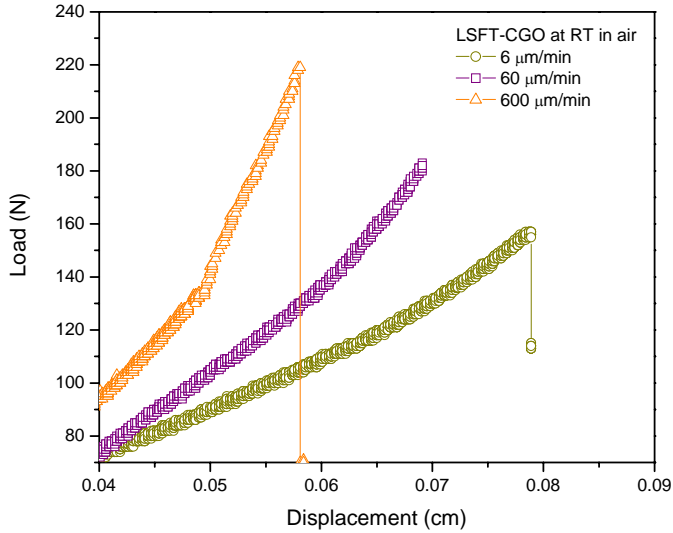| No.	Experimental Conditions	Cross Head Speed	Maximum Load (N)	Maximum Strength (MPa)
1.	RT, Air	6 μm/min	157	82.3
2	RT, Air	6 μm/min	133	53.2
3.	RT, Air	60 μm/min	182	104.8
4.	RT, Air	600 μm/min	219	90.8
5.	RT, Air	600 μm/min	201	94.1
6.	1000°C, in N_2	60 μm/min	120	51.2

Figure 9. Effect of strain rate on the fracture load.

The presence of a flaw such as a crack, pore, or inclusion in a ceramic material results in stress concentration. Griffth proposed an equation for the form

$$\sigma_f = A\left(\frac{E\,\gamma}{c} \right) \qquad \text{--- (2.2)}$$

for relating the fracture stress to the material properties and the flaw size, where σ_f is the fracture stress, E the elastic modulus, γ the fracture energy, c the flaw size, and A a constant that depends on the specimen and flaw geometries. In the slower strain rate the crack growth is relatively easier by linking up with the grain boundaries and neighboring flaws which eventually increase the size of the critical flaw and reduce the fracture stress. In the slower strain rate the slow crack growth facilitates the fracture at the lower applied stress itself. In the rapid loading, materials fail at higher fracture stress due to the absence of slow crack growth. Hence, the stress needed to fracture the LSFT-CGO at 600 µm/min is 25% higher than to fracture the membrane at 6 µm/min.

Bend strength in N_2 atmosphere at elevated temperatures:

The LSFT-CGO test specimen was loaded in the 4-point bend fixture and the N_2 was purged during heating of the autoclave. The temperature was maintained at 1000°C for 60min prior to apply any load. The specimen was loaded with a rate of 60 μm/min. The furnace power was switched off after the fracture of the sample. The load displacement curve is shown in Figure 10.
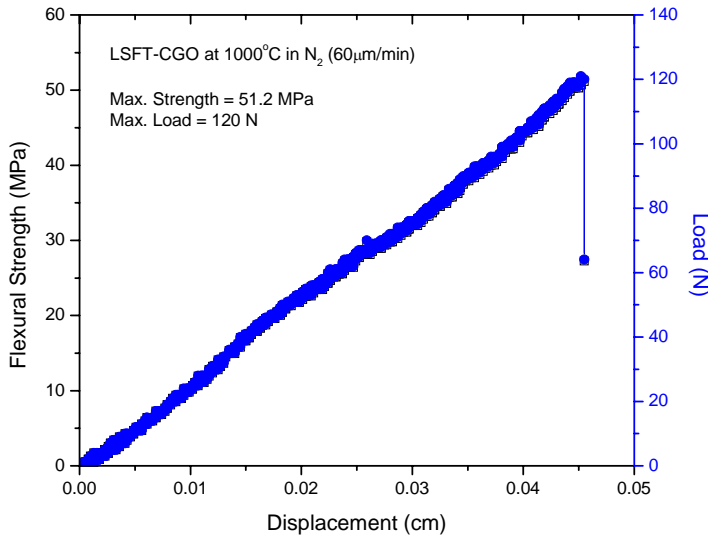

Figure 10. Bend strength of LSFT-CGO is at 1000°C in N_2 atmosphere.

The load increased monotonically with increasing displacement till the specimen failed at 120 N. The bend strength calculated was 51.2 MPa. LSFT-CGO had a higher bend strength at RT in air. Figure 7 shows the load-displacement plot for the bend strength test with the same loading rate. The reduction in the strength may be due to the development of new flaws or crack growth from the already existing flaws. The formation of oxygen deficiencies at high temperature can also cause the strength degradation. A detailed characterization of the fractured samples using XRD, SEM and TGDTA is planned. The bend strength tests at 1000°C in air also planned in the next quarter to understand the effect of temperature on LDFT-CGO.

It was identified from the bend strength experiments that the geometry plays an important role in achieving proper fracture of the sample. In some of the experiments the specimens failed closer to the 4-point bend ZrO_2 rollers (top). The

photographs of the fractured specimens are shown in Figure 11. The reason for such failures was identified as the improper alignment or geometry of the specimen. Hence, some of the test will be repeated to get the proper fracture.
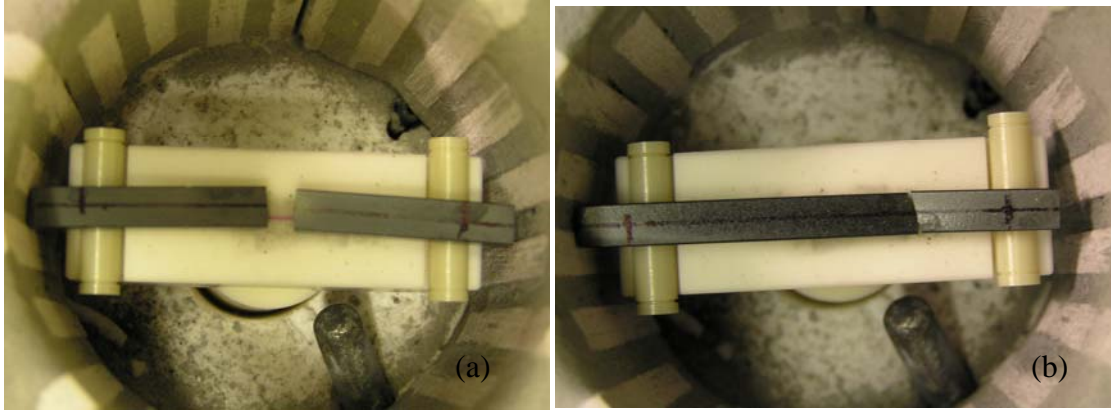

Figure 11. Fractured LSFT-CGO in RT in air. (a) Perfect failure at the center of the sample (b) Specimen failed at the ZrO_2 rollers due to uneven specimen geometry.

Plans for the next quarter:

1. Complete thermal analysis of the LSFT-CGO
2. Bend strength tests at 1000°C in air
3. Characterization of the fractured samples using XRD and SEM.

Measurement of Surface Activation/Reaction Rates in Ion Transport Membranes using Isotope Tracer and Transient Kinetic Techniques

A. J. Jacobson, University of Houston, C.A. Mims, University of Toronto

EXPERIMENTAL

We have investigated two different synthesis routes to GDC using either formate or carbonate precursors. Several procedures were investigated in order to obtain both the maximum yield of precursor and to produce homogeneous and small-sized crystals. The carbonate route used the approach of Fujihara *et al* who reported both the synthesis of cerium carbonate and samarium-doped cerium carbonate.[i] In their report, $Ce(NO_3)_3 \cdot 6H_2O$ and urea were dissolved in deionized water and the solution was heated at 80 °C for 24 h. $Ce_2O(CO_3)_2 \cdot H_2O$ was precipitated in the form of rod-shaped particles (approximately 5 x 2 µm) were obtained as a result of fast crystal growth in the solution. When $CeCl_3 \cdot 6H_2O$ was used instead of nitrate, triangular prism-shaped particles (approximately 20 – 30 µm in height and 5 – 10 µm in thickness) were precipitated.

The formate precursor $Ce(Gd)(HCOO)_3$ was synthesized from the nitrates by hydrolysis of dimethylformamide. All reactants were reagent-grade and were used as purchased without further purification. Cerium (III) nitrate hexahydrate ($Ce(NO_3)_3 \cdot 6H_2O$; 99%, Aldrich), gadolinium (III) nitrate hexahydrate ($Gd(NO_3)_3 \cdot 6H_2O$; 99.9 %, Aldrich). In typical syntheses $Ce(NO_3)_3 \cdot 6H_2O$ and $Gd(NO_3)_3 \cdot 6H_2O$ were dissolved in either $DMF/EtOH/H_2O$ or $DMF/HCOOH/H_2O$ and this solution was refluxed at 100 °C for 12 h to give needle-shaped white crystals of the formate. This method gave a high yield, c.a. 97%, with crystal size of ~15 µm long (Figure 12a). The formate was heat-treated at 350 ~ 400 °C for 12 h to give yellow CGO powder.

The carbonate precursor $(Ce,Gd)(CO_3)(OH)$ was prepared via a modification of the precipitation method used by Fujihara *et al.* Cerium nitrate and gadolinium nitrate were dissolved in deionized water in the ratio of Ce/Gd = 9/1. Urea (99+ %, Aldrich) was added to this solution. The reaction vessel was placed in a silicone oil bath and the solution was refluxed at 105 ˚C for 12 h with vigorous stirring. The product, a white

powder was filtered and washed with water and ethanol. Finally, the carbonate was heat-treated at 350 ~ 400 °C for 12 h to give yellow CGO powder.

Characterization.

The precursor and CGO particle morphologies were examined by scanning electron microscopy (SEM-JEOL 8300). The thermal decomposition behaviors of $Ce(Gd)(HCOO)_3$ and $Ce(Gd)(CO_3)(OH)$ were determined by thermogravimetric analysis (TGA) at a rate of $3°C/min$ in air using a V5.1A Du Pont 2100 instrument. The X-ray powder diffraction patterns of the precursor and CGO were collected on a Scintag XDS 2000 diffractometer with Cu$K\alpha$ radiation. Nitrogen adsorption isotherms were measured using COULTER OMISORP 100 automated gas sorption analyzer. Conductivity measurements were made by AC impedance spectroscopy on sintered disks in air using platinum electrodes.

RESULTS AND DISCUSSION

Formate precursor:

The large crystal size of the formate precursor does not lead to a powder that is easy to densify (see below). Consequently, the reaction conditions were modified in order to maintain a high yield but of smaller crystals. Reactions with a mixture of $Ce(NO_3)_3·6H_2O$ or $CeCl_3·6H_2O$ and $Gd(OAc)_3·xH_2O$ in DMF/EtOH/H$_2$O with and without formic acid was heated at 80 – 100 °C for 12 – 24 h. The yield of formate was less than 45 % with crystal sizes approximately 2 – 10 µm except when cerium chloride was used with formic acid at 100 °C, the yield was doubled than that from nitrate. When the reaction was carried out in a static reaction vessel such as a stainless bomb or sealed tube, the average crystal size was about 500 µm at 100 °C and 50 – 200 µm at 80 °C (Figure 12b). Attempts to make the particle size of CGO small by rapid heating the formate to 400 °C, quenching the heated sample, or using a surfactant (TritonX-100) in the initial synthesis, were unsuccessful.
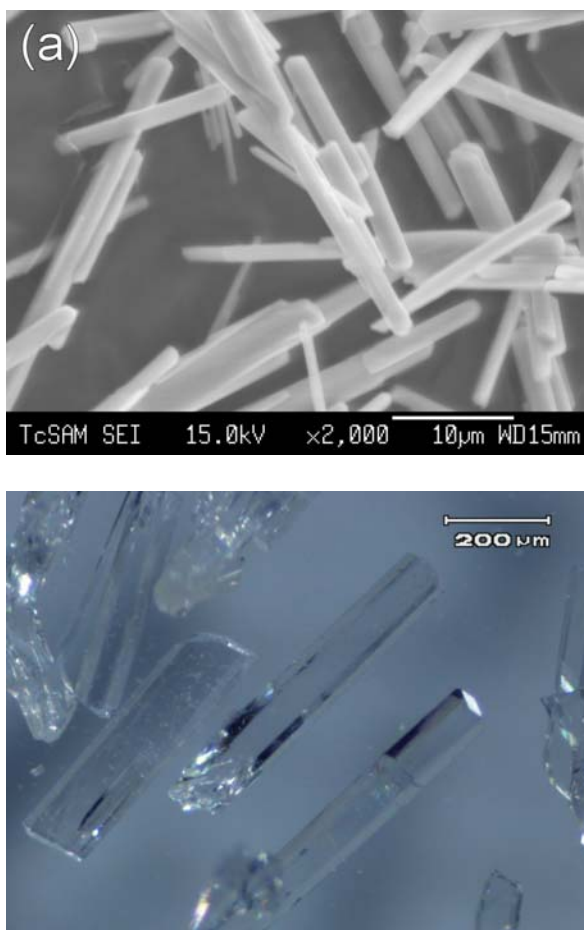
Fig. 12. Crystals of (Ce,Gd)(HCOO)$_3$ a) under reflux conditions, b) in static conditions.

Carbonate precursor:

Following the procedure described above with the concentration of metal ions and urea adjusted to 0.2 and 0.5M, reaction in either a stainless steel reactor with a Teflon liner or in a flask with a reflux condenser at 80 to 105 °C for 12 to 24 h gave a low yield of carbonate (~40 %) at $\geq$ 100 °C and a lower yield at lower temperatures. The use of cerium chloride instead of cerium nitrate under the same conditions did not improve the yield although the crystal size was ~ 2 – 3 µm compared to the larger formate crystals formed under similar conditions. (Figure 13a).
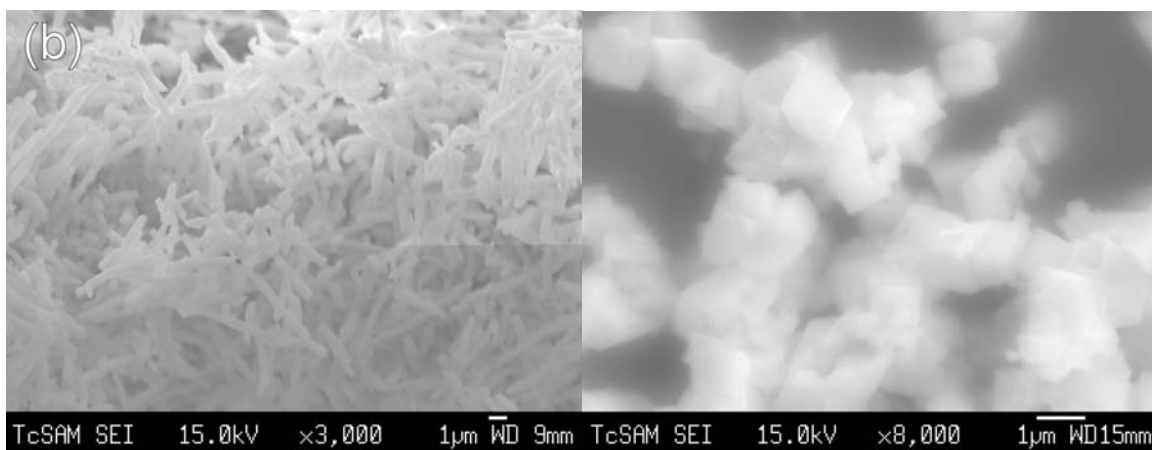
Fig. 13 Crystals of $(Ce,Gd)(CO_3)(OH)$ a) initial synthesis b) optimized (after decomposition).

In order to optimize the reaction conditions, the effects of varying the amount of urea and the temperature were examined systematically. The molar ratio of metal ions to urea was varied from 1:1 to 1:6 and the reaction mixture was heated at 80, 90, 95, 100, or 105 °C. When the ratio was 1:1 or 1:2, the yield was about 50 % regardless of the reaction temperature. When the ratio was more than 1:3 the yield increased to ~95 % with temperature until 95 °C. At the reaction temperature over 100 °C, the ratio of 1:3 gave a maximum yield of 99.9 %. The resulting carbonate crystals were small square blocks with dimensions of 1 x 1 x 0.5 µm (Fig. 13b).

Thermal decomposition:

The thermal decomposition behaviors of two precursors were examined by TGA (Fig. 14). The formate shows a one-step decomposition to CGO starting at 270 ℃ and complete at 315 ℃ (obs. 35.87 %, calcd. 37.22 %), while the decomposition of the carbonate starts at 230 ℃ and is complete at 280 ℃ (obs. 20.21 %, calcd. 20.25 %). The decomposition of these precursors to CGO is pseudomorphic (Fig. 15) in the sense that after the decomposition the gross morphology of the crystals is preserved.

A similar pseudomorphic decomposition of cerium hydroxycarbonate has been reported previously.[ii] It has also been noted that the morphology of the precursor can be changed; when the 9 – 14 µm carbonate was quenched from 500 or 800 °C, the particle size was reduced to 1.5 – 3 µm or 0.8 – 2 µm, respectively.[iii]
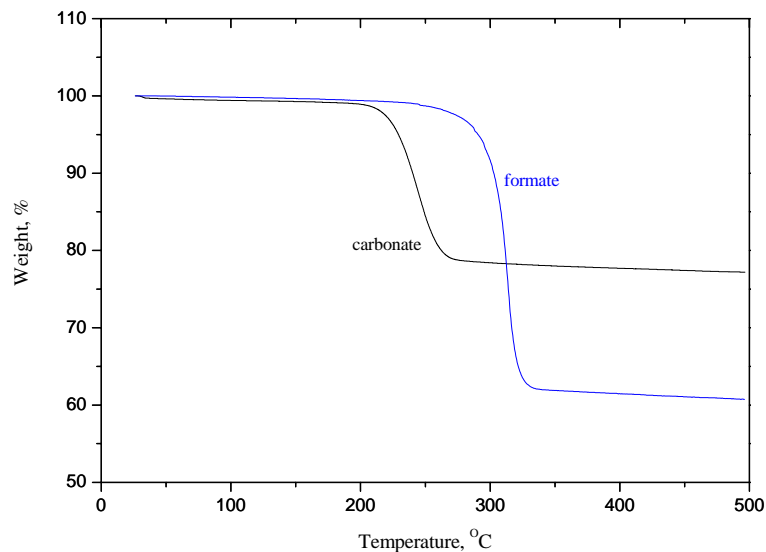
Fig. 14. TGA curves of the formate (solid line) and carbonate (dotted line) powders.

The pseudomorphic transformation of the precursors presents a problem for further powder processing when the initial crystals are large. As an example, an SEM micrograph of a formate crystal after decomposition is shown in Fig. 15. The overall shape of the crystal is little changed but numerous crack and fissures have appeared as a result of the gas evolution during conversion to CGO. Considerable additional efforts are required to convert the powder into a suitable form for densification and hence our efforts to reduce the crystal size o that shown in Fig. 13b.

The pseudomorphic transformation is also accompanied by the formation of a sample with significant surface area and relatively narrow pore size distribution as shown by the nitrogen adsorption isotherm in Fig. 15 obtained from sample of CGO obtained from the decomposition of formate after dehydration under vacuum at 250º C overnight. The total volume adsorbed is ca. 36 ml/g and the calculated BET surface area is 123 m^2/g.
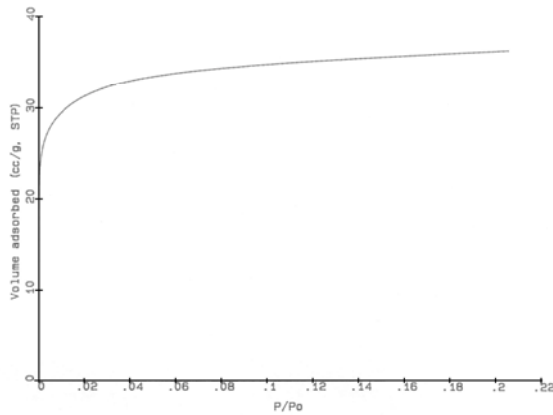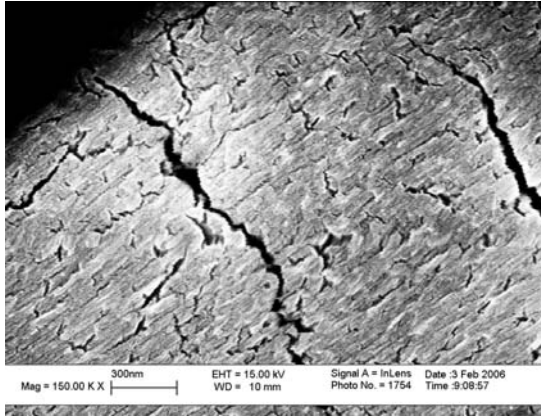
Fig. 15 a) SEM of CGO after heat treatment of a formate crystal at 350 ° C for 12h, b) N$_2$ gas sorption isotherm at 77 K for CGO.

*CGO conductivity***:**

The conductivity of the CGO electrolyte was measured by AC impedance spectroscopy. As shown in Fig. 16a, at 318 °C and at relatively high frequency (> 2 kHz), two distinctive semicircles with some distortion are observed and are associated with the grain and grain boundary response of the CGO electrolyte. As the operating temperature is increased (>400 °C), the two semi circles merge together and the grain and grain boundary processes cannot be completely separated.
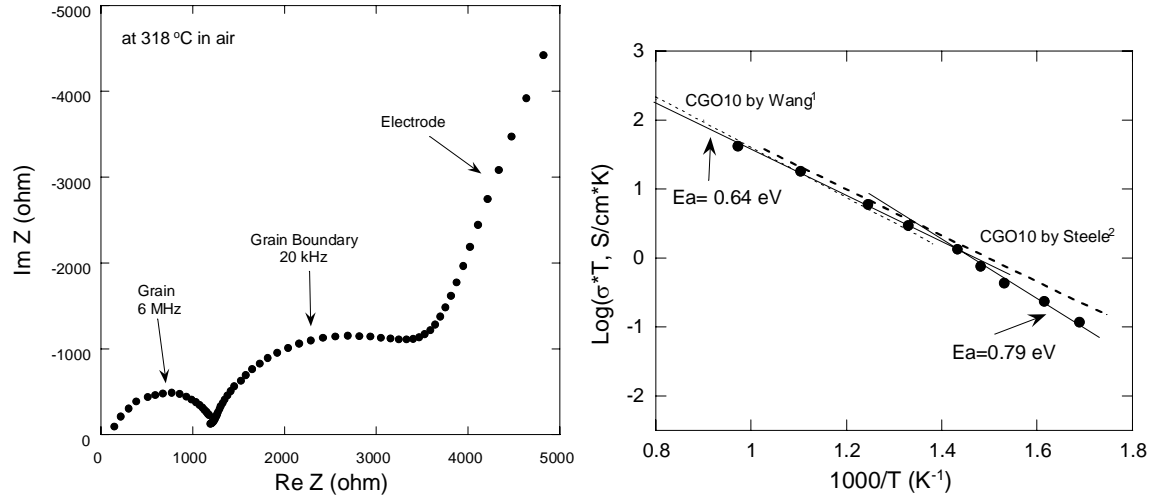
Fig. 16 a) Impedance spectrum CGO at 318 ^{o}C in air, b) comparison of the electrical conductivity vs. temperature for CGO10 with literature data.

The temperature dependence of the electrical conductivities of CGO prepared by the carbonate precursor route is shown in Fig 16b. The measured data are in good agreement with the data of CGO10 by other groups [iv] though the conductivity data measured by Steele et al. v are slightly higher at lower temperature. Furthermore, Steele [vi] reported that the conductivity shows a small change in slope around 400 °C which is associated with ($Gd_{Ce}^{'} - V_O^{''}$) complexes. Above 400 ^{o}C, the ($Gd_{Ce}^{'} - V_O^{''}$) complexes are dissociated, which gives rise to a lower activation energy of 0.64 eV than the activation energy of 0.79 eV at temperatures less than 400 ^{o}C (see Fig. 16b).

Plans for the Next Quarter.

In the next quarter we will continue densification studies of both La$_2$NiO$_4$ and PrBaCo$_2$O$_5$ composites with CGO. The initial compositions will use 25 and 50 % CGO to cover the range above and below the CGO percolation threshold. We will measure the thermal expansion coefficients of the composite materials. Assuming that dense samples can be prepared, we will then carry out permeation measurements. A new apparatus for this purpose has been constructed and tested during the last quarter.

CONCLUSIONS:

A non-agglomerated and nanocrystalline-sized powder was successfully produced using ethylene glycol nitrate methods. The LSFT powder prepared using this method exhibits well dispersed and nano sized particles about 100 – 200 nm and could be densified to 90% of its theoretical density. The LSFT sintered at 1400°C was not mechanically rigid and exhibited the evidence of a liquid phase at the grain boundaries. The electrical conductivity and Seebeck coefficient were measured as a function of temperature.

The effect of strain rate on the flexural strength of the LSFT-CGO test specimens was studied. Three strain rates 6, 60 and 600 μm/ min were chosen for this study. In the slower strain rate the slow crack growth facilitates the fracture at the lower applied stress itself. In the rapid loading, membrane fails at higher fracture stress due to the absence of slow crack growth. A reduction in the strength of the membrane was observed at 1000°C in N_2.

The GDC was synthesized using either formate or carbonate precursors. *The formate precursor* $Ce(Gd)(HCOO)_3$ was synthesized from the nitrates by hydrolysis of dimethylformamide. *The carbonate precursor* $(Ce,Gd)(CO_3)(OH)$ was prepared via a modification of the precipitation method. The precursor and CGO particle morphologies were examined by SEM and XRD. The thermal decomposition behaviors of $Ce(Gd)(HCOO)_3$ and $Ce(Gd)(CO_3)(OH)$ were determined by thermogravimetric analysis. Conductivity measurements were made by AC impedance spectroscopy on sintered disks in air using platinum electrodes.

LIST OF ACRONYMS AND ABBREVIATIONS

CGO	Cerium gadolinium oxide
GDC	Gadolinia doped ceria
YSZ	Yttria stabilized zirconia
XRD	X-ray diffraction

REFERENCES

[i]   M. Oikawa, S. Fujihara, J. Solid State Chem. 178 (2005) 2036.
[ii]   H.-C. Wang, C.-H. Lu, Mater. Res. Bull. 37 (2002) 783.
[iii]   Lu, C. H.; Wang, H. C. Mater. Sci. Eng. B90 (2002) 138.
[iv]   S. Wang, T. Kobayaxhi, M. Dokiya and T. Hashimoto, J. Electrochem. Soc., 147 (2000) 3606.
[v]   B. C. H. Steele and A. Heinzel, Nature 414 (2001) 345.
[vi]   B.C.H. Steele, Solid State Ionics 129 (2000) 95.